Two-dimensional thermal model of the finite-difference lattice Boltzmann method with high spatial isotropy

Minoru Watari* and Michihisa Tsutahara
Graduate School of Science and Technology, Kobe University, 1-1 Rokkodai, Nada, Kobe 657-8501, Japan
(Received 5 November 2002; published 26 March 2003)

The existing lattice Boltzmann method multispeed thermal models show a limited accuracy. This paper proposes a two-dimensional multispeed thermal model for the finite-difference lattice Boltzmann method (FDLBM). To recover correct fluid equations, up to fourth orders of local flow velocity should be retained in the local equilibrium distribution function and tensors of particle velocities should have up to seventh rank isotropy. In the FDLBM, particle velocities can be selected independently from the lattice configuration. Therefore, particle velocities of octagonal directions, which have up to seventh rank isotropic tensors, are adopted. The proposed model was verified by two simulations. The model showed excellent numerical stability in addition to strict accuracy.

DOI: 10.1103/PhysRevE.67.036306 PACS number(s): 47.11.+j, 51.10.+y

I. INTRODUCTION

The lattice Boltzmann method (LBM) has become a powerful numerical tool for simulating fluid flows [1]. In the LBM, there are two ways of handling thermal fluids. One is the so-called ''multicomponent thermal model'' [2], where heat is handled as a different component from fluid. This model characterizes the flow as a Boussinesq fluid. Another is the so-called ''multispeed thermal model'' [3,4], where several particle velocities that have different speeds are used. While the multispeed thermal model is intended to correctly represent heat characteristics and compressibility, the existing models seem to have hidden error terms and show a limited accuracy.

The finite-difference lattice Boltzmann method (FDLBM) [5] was proposed in order to secure numerical stability and to apply nonuniform grids. In the LBM, the particle velocities are restricted to those that exactly link the lattice nodes in unit time. On the other hand, in the FDLBM as we do not need to consider that constraint, we can select particle velocities independently from the lattice configuration. Therefore, we can construct a correct and numerically stable multispeed thermal model by adopting more isotropic particle velocities. We propose in this paper a two-dimensional FDLBM BGK (single relaxation) thermal model based on the above concept.

II. FINITE-DIFFERENCE LATTICE BOLTZMANN METHOD

Below is a general description of the two-dimensional FDLBM thermal model. The evolution of the distribution function f_{ki} for the particle velocity $\mathbf{c}_{ki}$ is governed by the following equation:

$$\frac{\partial f_{ki}}{\partial t}+c_{ki\alpha}\frac{\partial f_{ki}}{\partial r_\alpha}=-\frac{1}{\phi}(f_{ki}-f_{ki}^{(0)}), \tag{1}$$

where subscript k indicates a group of the particle velocities whose speed is c_k and i indicates the particle's direction. The subscript α indicates x or y component. The variable t is time, r_α is the spatial coordinate, $f_{ki}^{(0)}$ is the local equilibrium distribution function, and ϕ is the relaxation parameter. The macroscopic quantities, density ρ, velocity u_α, and internal energy e, are defined as

$$\rho=\sum_{ki} f_{ki}, \tag{2}$$

$$\rho u_\alpha=\sum_{ki} f_{ki}c_{ki\alpha}, \tag{3}$$

$$\rho\left(e+\frac{u^2}{2}\right)=\sum_{ki} f_{ki}\frac{c_k^2}{2}. \tag{4}$$

The local equilibrium distribution function is determined to satisfy the following moment summation equations:

$$\sum_{ki} f_{ki}^{(0)}=\rho, \tag{5}$$

$$\sum_{ki} f_{ki}^{(0)}c_{ki\alpha}=\rho u_\alpha, \tag{6}$$

$$\sum_{ki} f_{ki}^{(0)}c_{ki\alpha}c_{ki\beta}=\rho(e\delta_{\alpha\beta}+u_\alpha u_\beta), \tag{7}$$

$$\sum_{ki} f_{ki}^{(0)}c_{ki\alpha}c_{ki\beta}c_{ki\gamma}=\rho[e(u_\alpha\delta_{\beta\gamma}+u_\beta\delta_{\gamma\alpha}+u_\gamma\delta_{\alpha\beta}) + u_\alpha u_\beta u_\gamma], \tag{8}$$

$$\sum_{ki} f_{ki}^{(0)}\frac{c_k^2}{2}=\rho\left(e+\frac{u^2}{2}\right), \tag{9}$$

$$\sum_{ki} f_{ki}^{(0)}\frac{c_k^2}{2}c_{ki\alpha}=\rho u_\alpha\left(2e+\frac{u^2}{2}\right), \tag{10}$$

*Electronic address: watari@mi-1.scitec.kobe-u.ac.jp

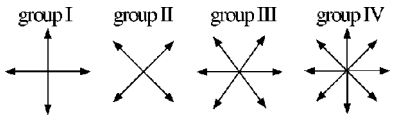

FIG. 1. Four groups of particle velocities.

$$\sum_{ki} f_{ki}^{(0)} \frac{c_k^2}{2} c_{ki\alpha} c_{ki\beta} = \rho \left[e\left(2e + \frac{u^2}{2} \right) \delta_{\alpha\beta} + u_\alpha u_\beta \left(3e + \frac{u^2}{2} \right) \right]. \tag{11}$$

By applying the Chapman Enskog expansion, the above formulation is shown to be equivalent, with no errors, to the following fluid equations (Navier-Stokes equations):

$$\frac{\partial \rho}{\partial t} + \frac{\partial}{\partial r_\alpha}(\rho u_\alpha) = 0, \tag{12}$$

$$\frac{\partial}{\partial t}(\rho u_\alpha) + \frac{\partial}{\partial r_\beta}(\rho u_\alpha u_\beta + P\delta_{\alpha\beta}) - \frac{\partial}{\partial r_\beta}\left[\mu \left(\frac{\partial u_\beta}{\partial r_\alpha} + \frac{\partial u_\alpha}{\partial r_\beta} - \frac{\partial u_\gamma}{\partial r_\gamma}\delta_{\alpha\beta} \right) \right] = 0, \tag{13}$$

$$\frac{\partial}{\partial t}\left[\rho \left(e + \frac{u^2}{2} \right) \right] + \frac{\partial}{\partial r_\alpha}\left[\rho u_\alpha \left(e + \frac{u^2}{2} + \frac{P}{\rho} \right) \right] - \frac{\partial}{\partial r_\alpha}\left[\kappa' \frac{\partial e}{\partial r_\alpha} + \mu u_\beta \left(\frac{\partial u_\beta}{\partial r_\alpha} + \frac{\partial u_\alpha}{\partial r_\beta} - \frac{\partial u_\gamma}{\partial r_\gamma}\delta_{\alpha\beta} \right) \right] = 0, \tag{14}$$

where pressure P, viscosity coefficient μ, and heat conductivity κ' have the following relations:

$$P = \rho e, \tag{15}$$

$$\mu = \rho e \phi, \tag{16}$$

$$\kappa' = 2\rho e \phi. \tag{17}$$

Temperature T is related with the internal energy by the following equation (R is gas constant):

$$T = e/R. \tag{18}$$

III. NEW FDLBM MODEL DERIVATION

The nth rank tensor for the group of m particle velocities is defined as

$$E^{(n)}_{\alpha_1\alpha_2\alpha_3\cdots\alpha_n} = \sum_{i=1}^{m} c_{i\alpha_1} c_{i\alpha_2} c_{i\alpha_3} \cdots c_{i\alpha_n}, \tag{19}$$

where $\alpha_1 \cdots \alpha_n$ indicates either x or y component. The tensor is isotropic if it is invariant for the coordinate rotation and the reflection. As for being isotropic, the odd rank tensors should vanish and the even rank tensors should be the sum of all possible products of Kronecker delta [6].

The tensors for four groups of particle velocities shown in Fig. 1 are summarized in Table I. Kronecker delta $\delta_{\alpha\beta}$ and the sum of its products, $\Delta_{\alpha\beta\gamma\chi}$ and $\Delta_{\alpha\beta\gamma\chi\lambda\tau}$, are isotropic, whereas extended Kronecker delta $\delta_{\alpha\beta\gamma\chi}$ and $\delta_{\alpha\beta\gamma\chi\lambda\tau}$ are anisotropic.

The odd tensors for uniformly distributed velocities are shown to vanish. For even tensors, groups I and II yield anisotropic tensors for the fourth rank and higher. Group III ensures isotropy up to the fourth rank, but not for higher ranks. However, group IV ensures isotropy up to the seventh rank.

The energy diffusion equation (11) contains up to fourth order of flow velocity u. Consequently, we derive the local equilibrium distribution function $f_{ki}^{(0)}$ as the polynomial form of flow velocity from the Maxwellian distribution:

$$\frac{\rho}{2\pi e}\exp\left[-\frac{1}{2e}(c_{ki\xi} - u_\xi)^2 \right] = \rho \frac{1}{2\pi e}\exp\left(-\frac{1}{2e}c_k^2 \right)\exp\left[\frac{1}{e}\left(c_{ki\xi}u_\xi - \frac{u^2}{2} \right) \right], \tag{20}$$

retaining up to fourth order terms of flow velocity

$$f_{ki}^{(0)} = \rho F_k \left[\left(1 - \frac{u^2}{2e} + \frac{u^4}{8e^2} \right) + \frac{1}{e}\left(1 - \frac{u^2}{2e} \right) c_{ki\xi}u_\xi + \frac{1}{2e^2}\left(1 - \frac{u^2}{2e} \right) c_{ki\xi}c_{ki\eta}u_\xi u_\eta + \frac{1}{6e^3} c_{ki\xi}c_{ki\eta}c_{ki\zeta}u_\xi u_\eta u_\zeta + \frac{1}{24e^4} c_{ki\xi}c_{ki\eta}c_{ki\zeta}c_{ki\chi}u_\xi u_\eta u_\zeta u_\chi \right], \tag{21}$$

where the parameter F_k represents $(1/2\pi e)\exp[-(1/2e)c_k^2]$ and is a function of e and c_k. The local equilibrium distribution function $f_{ki}^{(0)}$ contains the fourth rank tensor and the momentum diffusion equation (8) contains the third rank tensor. Therefore, up to seventh rank tensor should be isotropic to recover the correct fluid equations.

When we apply the property that the odd tensors vanish, we obtain the following equations to determine the parameters F_k.

From Eq. (5),

$$\sum_{ki} F_k = 1, \tag{22}$$

$$\sum_{ki} F_k c_{ki\xi} c_{ki\zeta} u_\xi u_\zeta = e u^2, \tag{23}$$

$$\sum_{ki} F_k c_{ki\xi} c_{ki\zeta} c_{ki\eta} c_{ki\chi} u_\xi u_\zeta u_\eta u_\chi = 3e^2 u^4. \tag{24}$$

TABLE I. Tensors for four groups shown in Fig. 1 $\delta_{\alpha\beta}=1$ if $\alpha=\beta$ and 0 otherwise, $\delta_{\alpha\beta\gamma\chi}=1$ if $\alpha=\beta=\gamma=\chi$ and 0 otherwise, $\delta_{\alpha\beta\gamma\chi\lambda\tau}=1$ if $\alpha=\beta=\gamma=\chi=\lambda=\tau$ and 0 otherwise, $\Delta_{\alpha\beta\gamma\chi}=\delta_{\alpha\beta}\delta_{\gamma\chi}+\delta_{\alpha\gamma}\delta_{\beta\chi}+\delta_{\alpha\chi}\delta_{\beta\gamma}$, $\Delta_{\alpha\beta\gamma\chi\lambda\tau}=\delta_{\alpha\beta}\Delta_{\gamma\chi\lambda\tau}+\delta_{\alpha\gamma}\Delta_{\beta\chi\lambda\tau}+\delta_{\alpha\chi}\Delta_{\beta\gamma\lambda\tau}+\delta_{\alpha\lambda}\Delta_{\beta\gamma\chi\tau}+\delta_{\alpha\tau}\Delta_{\beta\gamma\chi\lambda}$. Kronecker delta $\delta_{\alpha\beta}$ and the sum of its products, $\Delta_{\alpha\beta\gamma\chi}$ and $\Delta_{\alpha\beta\gamma\chi\lambda\tau}$, are isotropic, whereas extended Kronecker delta $\delta_{\alpha\beta\gamma\chi}$ and $\delta_{\alpha\beta\gamma\chi\lambda\tau}$ are anisotropic. The c_k is the speed of the group of velocities. The odd tensors for any groups are zero (isotropic).

Group	$\Sigma_i c_{ki\alpha}c_{ki\beta}$	$\Sigma_i c_{ki\alpha}c_{ki\beta}c_{ki\gamma}c_{ki\chi}$	$\Sigma_i c_{ki\alpha}c_{ki\beta}c_{ki\gamma}c_{ki\chi}c_{ki\lambda}c_{ki\tau}$
Group I	$2c_k^2\delta_{\alpha\beta}$	$2c_k^4\delta_{\alpha\beta\gamma\chi}$	$2c_k^6\delta_{\alpha\beta\gamma\chi\lambda\tau}$
Group II	$2c_k^2\delta_{\alpha\beta}$	$c_k^4\Delta_{\alpha\beta\gamma\chi}-2c_k^4\delta_{\alpha\beta\gamma\chi}$	$c_k^6\Delta_{\alpha\beta\gamma\chi\lambda\tau}/6-2c_k^6\delta_{\alpha\beta\gamma\chi\lambda\tau}$
Group III	$3c_k^2\delta_{\alpha\beta}$	$3c_k^4\Delta_{\alpha\beta\gamma\chi}/4$	anisotropic
Group IV	$4c_k^2\delta_{\alpha\beta}$	$c_k^4\Delta_{\alpha\beta\gamma\chi}$	$c_k^6\Delta_{\alpha\beta\gamma\chi\lambda\tau}/6$

From Eq. (6),

$$\sum_{ki} F_k c_{ki\alpha}c_{ki\xi}u_\xi = e u_\alpha, \tag{25}$$

$$\sum_{ki} F_k c_{ki\alpha}c_{ki\xi}c_{ki\zeta}c_{ki\eta}u_\xi u_\zeta u_\eta = 3e^2u^2u_\alpha. \tag{26}$$

From Eq. (7),

$$\sum_{ki} F_k c_{ki\alpha}c_{ki\beta} = e\,\delta_{\alpha\beta}, \tag{27}$$

$$\sum_{ki} F_k c_{ki\alpha}c_{ki\beta}c_{ki\xi}c_{ki\zeta}u_\xi u_\zeta = e^2(u^2\delta_{\alpha\beta}+2u_\alpha u_\beta), \tag{28}$$

$$\sum_{ki} F_k c_{ki\alpha}c_{ki\beta}c_{ki\xi}c_{ki\zeta}c_{ki\eta}c_{ki\chi}u_\xi u_\zeta u_\eta u_\chi = 3e^3u^2(u^2\delta_{\alpha\beta}+4u_\alpha u_\beta). \tag{29}$$

From Eq. (8),

$$\sum_{ki} F_k c_{ki\alpha}c_{ki\beta}c_{ki\gamma}c_{ki\xi}u_\xi = e^2(u_\alpha\delta_{\beta\gamma}+u_\beta\delta_{\gamma\alpha}+u_\gamma\delta_{\alpha\beta}), \tag{30}$$

$$\sum_{ki} F_k c_{ki\alpha}c_{ki\beta}c_{ki\gamma}c_{ki\xi}c_{ki\zeta}c_{ki\eta}u_\xi u_\zeta u_\eta = 3e^3u^2(u_\alpha\delta_{\beta\gamma}+u_\beta\delta_{\gamma\alpha}+u_\gamma\delta_{\alpha\beta})+6e^3u_\alpha u_\beta u_\gamma. \tag{31}$$

From Eq. (9),

$$\sum_{ki} F_k \frac{c_k^2}{2} = e, \tag{32}$$

$$\sum_{ki} F_k \frac{c_k^2}{2} c_{ki\xi}c_{ki\zeta}u_\xi u_\zeta = 2e^2u^2, \tag{33}$$

$$\sum_{ki} F_k \frac{c_k^2}{2} c_{ki\xi}c_{ki\zeta}c_{ki\eta}c_{ki\chi}u_\xi u_\zeta u_\eta u_\chi = 9e^3u^4. \tag{34}$$

From Eq. (10),

$$\sum_{ki} F_k \frac{c_k^2}{2} c_{ki\alpha}c_{ki\xi}u_\xi = 2e^2u_\alpha, \tag{35}$$

$$\sum_{ki} F_k \frac{c_k^2}{2} c_{ki\alpha}c_{ki\xi}c_{ki\zeta}c_{ki\eta}u_\xi u_\zeta u_\eta = 9e^3u^2u_\alpha. \tag{36}$$

From Eq. (11),

$$\sum_{ki} F_k \frac{c_k^2}{2} c_{ki\alpha}c_{ki\beta} = 2e^2\delta_{\alpha\beta}, \tag{37}$$

$$\sum_{ki} F_k \frac{c_k^2}{2} c_{ki\alpha}c_{ki\beta}c_{ki\xi}c_{ki\zeta}u_\xi u_\zeta = 3e^3(u^2\delta_{\alpha\beta}+2u_\alpha u_\beta), \tag{38}$$

$$\sum_{ki} F_k \frac{c_k^2}{2} c_{ki\alpha}c_{ki\beta}c_{ki\xi}c_{ki\zeta}c_{ki\eta}c_{ki\chi}u_\xi u_\zeta u_\eta u_\chi = 12e^4(u^4\delta_{\alpha\beta}+4u^2u_\alpha u_\beta). \tag{39}$$

If we further assume the application of group IV particle velocities that have isotropic tensors up to seventh rank, the above 18 equations reduce to the following five equations. From Eq. (22),

$$\sum_{ki} F_k = 1. \tag{40}$$

From Eqs. (23), (25), (27), and (32),

$$\sum_{ki} F_k c_k^2 = \frac{e}{4}. \tag{41}$$

From Eqs. (24), (26), (28), (30), (33), (35), and (37),

$$\sum_{ki} F_k c_k^4 = e^2. \tag{42}$$

From Eqs. (29), (31), (34), (36), and (38),

$$\sum_{ki} F_k c_k^6 = 6e^3. \tag{43}$$

From Eq. (39),

$$\sum_{ki} F_k c_k^8 = 48e^4. \tag{44}$$

Five speeds of particle velocities are necessary to satisfy the above equations. We assume a rest particle ($c_0=0.0$) and four speeds of group IV particles whose speeds are c_1, c_2, c_3, and c_4. Eqs. (40)–(44) are easily solved to give the following. The parameters F_k are functions of c_1, c_2, c_3, c_4, and internal energy e.

$$F_1=\frac{1}{c_1^2(c_1^2-c_2^2)(c_1^2-c_3^2)(c_1^2-c_4^2)}\left[48e^4-6(c_2^2+c_3^2+c_4^2)e^3 + (c_2^2c_3^2+c_3^2c_4^2+c_4^2c_2^2)e^2-\frac{c_2^2c_3^2c_4^2}{4}e\right], \tag{45}$$

$$F_2=\frac{1}{c_2^2(c_2^2-c_3^2)(c_2^2-c_4^2)(c_2^2-c_1^2)}\left[48e^4-6(c_3^2+c_4^2+c_1^2)e^3 + (c_3^2c_4^2+c_4^2c_1^2+c_1^2c_3^2)e^2-\frac{c_3^2c_4^2c_1^2}{4}e\right], \tag{46}$$

$$F_3=\frac{1}{c_3^2(c_3^2-c_4^2)(c_3^2-c_1^2)(c_3^2-c_2^2)}\left[48e^4-6(c_4^2+c_1^2+c_2^2)e^3 + (c_4^2c_1^2+c_1^2c_2^2+c_2^2c_4^2)e^2-\frac{c_4^2c_1^2c_2^2}{4}e\right], \tag{47}$$

$$F_4=\frac{1}{c_4^2(c_4^2-c_1^2)(c_4^2-c_2^2)(c_4^2-c_3^2)}\left[48e^4-6(c_1^2+c_2^2+c_3^2)e^3 + (c_1^2c_2^2+c_2^2c_3^2+c_3^2c_1^2)e^2-\frac{c_1^2c_2^2c_3^2}{4}e\right], \tag{48}$$

$$F_0=1-8(F_1+F_2+F_3+F_4). \tag{49}$$

As far as a simulation being stably conducted, the combination of values c_1, c_2, c_3, and c_4 does not affect the accuracy itself. We utilize this freedom to obtain the stably simulated range of temperature as wide as possible. Several criteria were tried and we finally concluded that following hypothesis has the closest relation with simulation stability: "Simulation is stable as far as $F_0>F_1>F_2>F_3>F_4>0$." Therefore, the following optimum problem was solved:

$$\begin{aligned}
&\text{Under the condition} && 0<c_1<c_2<c_3<c_4,\\
&\text{determine} && c_1, c_2, c_3, \text{ and } c_4,\\
&\text{which maximizes} && (e_H-e_L)/e_M,\\
&\text{for } e_L<e<e_H, && F_0/F_1>1.1,\\
& && F_1/F_2>1.1,\\
& && F_2/F_3>1.1,\\
& && F_3/F_4>1.1, \text{ and}\\
& && F_4>0 \text{ hold,}\\
&\text{keeping} && e_M=(e_H+e_L)/2=1.0,
\end{aligned} \tag{50}$$

where e_L, e_H, and e_M are, respectively, the lowest, the highest, and the middle internal energy of a stable simulation range.

The result of the optimization is the following. The model is expected to stably simulate flows for the temperature range: $e=0.4\sim1.6$.

$$(c_0, c_1, c_2, c_3, c_4)=(0.0, 1.0, 1.92, 2.99, 4.49), \tag{51}$$

$$e_L=0.4, \quad e_H=1.6, \quad (e_H-e_L)/e_M=1.2. \tag{52}$$

IV. VERIFICATION OF THE NEW MODEL

We confirmed validity of the model by conducting numerical simulations. First, the speed of sound was measured. Second, the shear flow between the parallel walls (Couette flow) was investigated.

The evolution equation (1) is solved by using the Euler and the second upwind difference scheme. The distribution function of next step f_{ki}^{new} is calculated as

$$f_{ki}^{new}=f_{ki}-\left(c_{kix}\frac{\partial f_{ki}}{\partial x}+c_{kiy}\frac{\partial f_{ki}}{\partial y}\right)\Delta t-\frac{1}{\phi}(f_{ki}-f_{ki}^{(0)})\Delta t, \tag{53}$$

$$\frac{\partial f_{ki}}{\partial x}=\begin{cases}\dfrac{3f_{ki,I}-4f_{ki,I-1}+f_{ki,I-2}}{2\Delta x} & \text{if } c_{kix}\geqslant 0\\[2ex] \dfrac{3f_{ki,I}-4f_{ki,I+1}+f_{ki,I+2}}{-2\Delta x} & \text{if } c_{kix}<0,\end{cases} \tag{54}$$

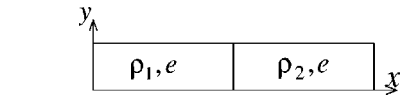

FIG. 2. Sound wave simulation. A plate divides fluids that have small differences in density. As the plate is removed, sound waves (expansion or compression) propagate in both directions.

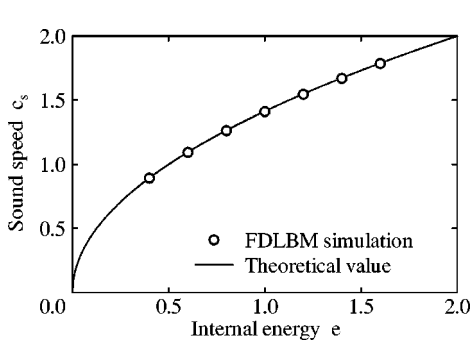

FIG. 3. Sound speed vs internal energy. The results are compared with the theoretical value: $c_s=\sqrt{2e}$.

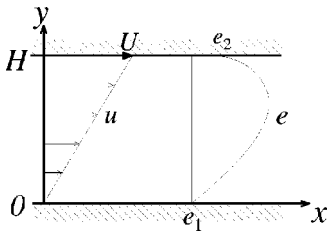

FIG. 4. Couette flow simulation. The upper wall, which is H apart from the lower wall and has an internal energy e_2, starts to move with a speed U. The lower wall has e_1 and is at rest.

$$\frac{\partial f_{ki}}{\partial y}=\begin{cases}\dfrac{3f_{ki,J}-4f_{ki,J-1}+f_{ki,J-2}}{2\Delta y} & \text{if } c_{kiy}\geqslant 0\\[2ex] \dfrac{3f_{ki,J}-4f_{ki,J+1}+f_{ki,J+2}}{-2\Delta y} & \text{if } c_{kiy}<0,\end{cases} \tag{55}$$

where the second suffixes $I-2$, $I-1$, I, $I+1$, and $I+2$ indicate the mesh nodes in x direction and $J-2$, $J-1$, J, $J+1$, and $J+2$ in y direction.

A. Speed of sound

In a box, as shown in Fig. 2, a plate divides fluids that have small difference in density. When the plate is removed, sound waves (expansion and compression) propagate. The position of the pressure jump was measured to calculate the speed of sound. The results at various internal energy levels are shown in Fig. 3. The simulation was stably conducted for the range: $e=0.4\sim1.6$. The speed of sound exactly agrees with the following theoretical value:

$$c_s=\sqrt{2e}. \tag{56}$$

B. Couette flow

A sketch of the simulation is shown in Fig. 4. The upper wall, which is H apart from the lower wall and has internal energy e_2, starts to move with a speed U. The lower wall has e_1 and is at rest. The viscous shear stress transmits momentum into the fluid and changes the horizontal speed profile. The horizontal speed distribution at various instants for $e_1=e_2$ is shown in Fig. 5. The simulation result exactly agrees with the following analytical value:

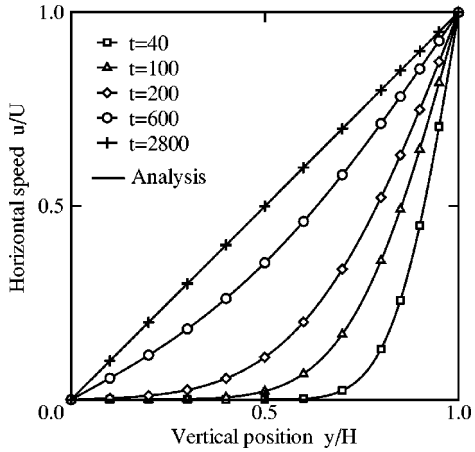

FIG. 5. Horizontal speed distribution for $e_1=e_2=1.0$ at various instants: $t=40$, 100, 200, 600, 2800.

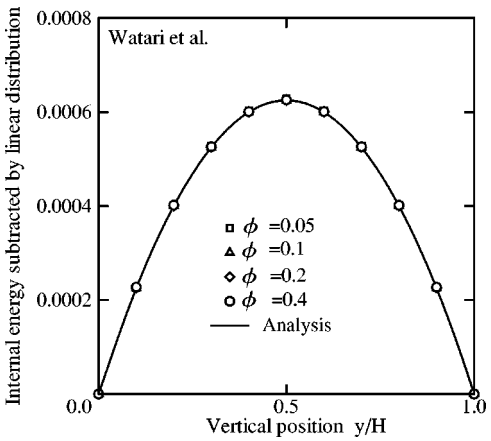

FIG. 6. Internal energy at steady state for $U=0.1$ and $e_1=e_2=1.0$. The internal energy subtracted by linear distribution is shown. The relaxation parameter is changed: $\phi=0.05$, 0.1, 0.2, 0.4. The results for all ϕ overlap each other.

$$\frac{u}{U}=\frac{y}{H}-\frac{2}{\pi}\sum_{n=1}^{\infty}\exp\left[-n^2\pi^2\frac{\mu t}{\rho H^2}\right]\sin\left[n\pi\left(1-\frac{y}{H}\right)\right]. \tag{57}$$

The analytical distribution of internal energy in a steady state is given as

$$e=e_1+(e_2-e_1)\frac{y}{H}+\frac{\mu}{2\kappa'}U^2\frac{y}{H}\left(1-\frac{y}{H}\right). \tag{58}$$

Since the coefficients μ and κ' are given as Eqs. (16) and (17), respectively, the value $\mu/2\kappa'$ is constant ($=0.25$). Therefore, the distribution does not depend on the relaxation

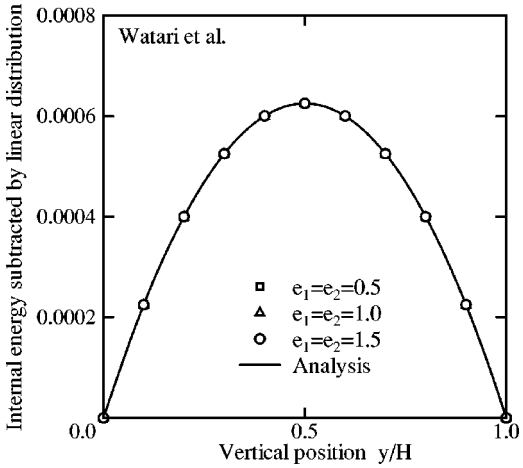

FIG. 7. Internal energy at steady state for $U=0.1$ and $\phi=0.1$. The internal energy subtracted by linear distribution is shown. The wall temperature is changed: $e_1=e_2=0.5$,1.0,1.5. The results for all cases overlap each other.

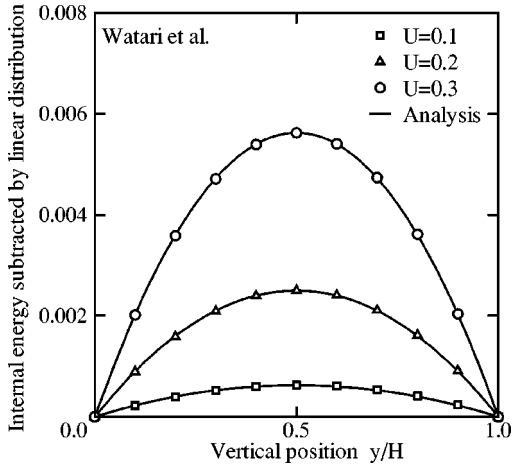

FIG. 8. Internal energy at steady state for different wall temperatures: $e_1=0.5, e_2=1.5$, and $\phi=0.1$. The internal energy subtracted by linear distribution is shown. The wall speed is changed: $U=0.1, 0.2, 0.3$.

parameter ϕ or on the wall's temperature. The internal energy subtracted by the linear distribution, which corresponds to the last term in Eq. (58), will be shown.

Figure 6 shows the result for various relaxation parameters. The result, which is independent of ϕ, conincides exactly with the analysis. Figure 7, the result for various wall temperatures, also shows complete agreement with the analysis.

Finally, we conducted simulations for $e_1 \neq e_2$. The result for various wall speeds and for $e_1=0.5$ and $e_2=1.5$ is shown in Fig. 8. The result exactly agrees with the analytical solution.

V. COMPARISON WITH EXISTING THERMAL MODELS

We conducted Couette simulations using existing multispeed thermal BGK LBM models in the same FDLBM scheme to compare them with the proposed model.

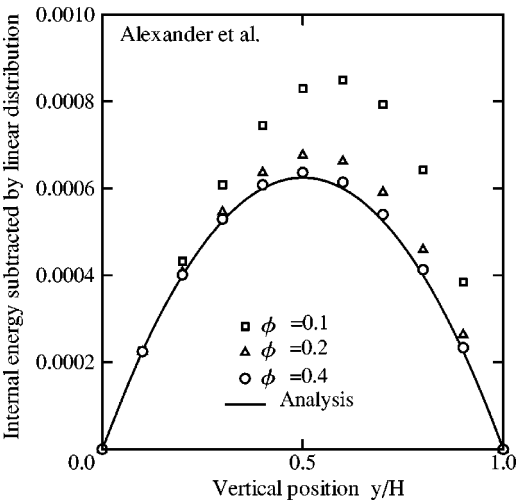

FIG. 9. Alexander's model. Internal energy at steady state for $U=0.1$ and $e_1=e_2=0.5$. The internal energy subtracted by linear distribution is shown. The relaxation parameter is changed: $\phi=0.1, 0.2, 0.4$. The result shows dependence on ϕ, which contradicts the analytical prediction.

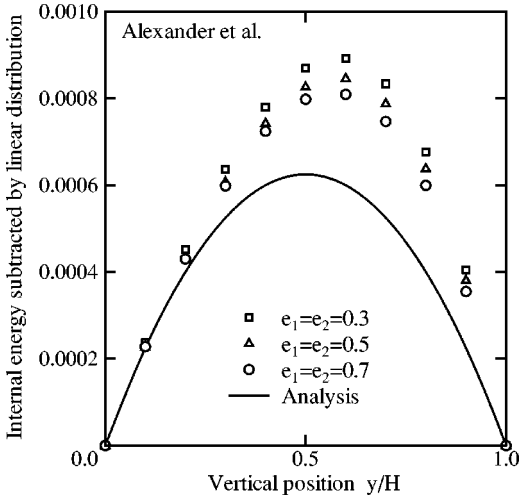

FIG. 10. Alexander's model. Internal energy at steady state for $U=0.1$ and $\phi=0.1$. The internal energy subtracted by linear distribution is shown. The wall temperature is changed: $e_1=e_2=0.3, 0.5, 0.7$. The result shows dependence on the wall temperature, which contradicts the analytical prediction.

The model by Alexander *et al*. 2D13V (one rest particle and two speeds of group III) [3]. They retain up to third orders of local flow speed in the local equilibrium distribution function. They use group III velocities (hexagonal) that ensure only fourth rank tensor isotropy. As we showed in the model derivation, up to fourth order expansion and up to seventh rank isotropy are necessary to recover correct fluid equations. Therefore, in their model, error terms are hidden in the momentum and energy diffusions. Figure 9 shows the result for the variation of the relaxation parameter. The result indicates the dependency on the relaxation parameter, which contradicts the analysis. The result for various values of the wall temperature is shown in Fig. 10. The figure shows the

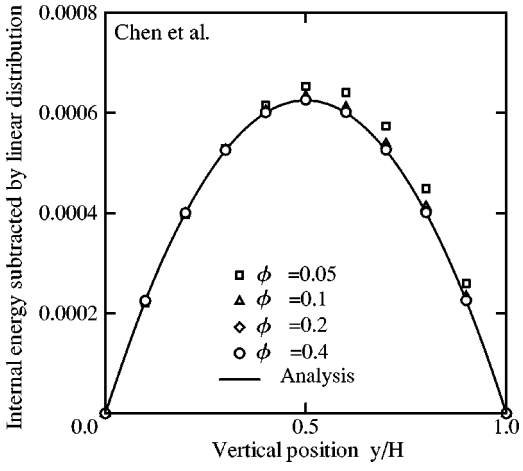

FIG. 11. Chen's model. Internal energy at steady state for $U=0.1$ and $e_1=e_2=0.5$. The internal energy subtracted by linear distribution is shown. The relaxation parameter is changed: $\phi=0.05, 0.1, 0.2, 0.4$. Although the model has been improved from Alexander's model, the result still shows dependence on ϕ, which contradicts the analytical prediction.

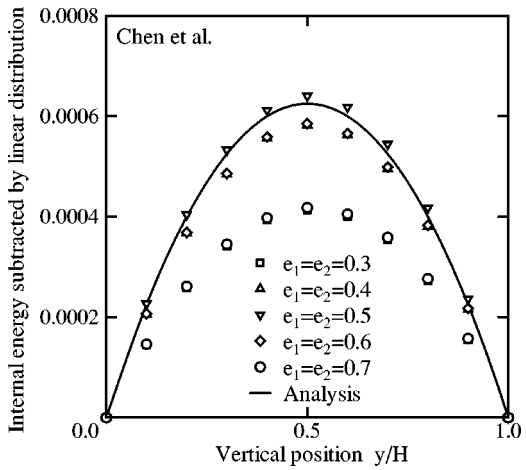

FIG. 12. Chen's model. Internal energy at steady state for $U=0.1$ and $\phi=0.1$. The internal energy subtracted by linear distribution is shown. The wall temperature is changed: $e_1=e_2=0.3, 0.4, 0.5, 0.6, 0.7$. The results for $e=0.4$ and 0.6 and for $e=0.3$ and 0.7 overlap. The result shows dependence on the wall temperature, which contradicts the analytical prediction.

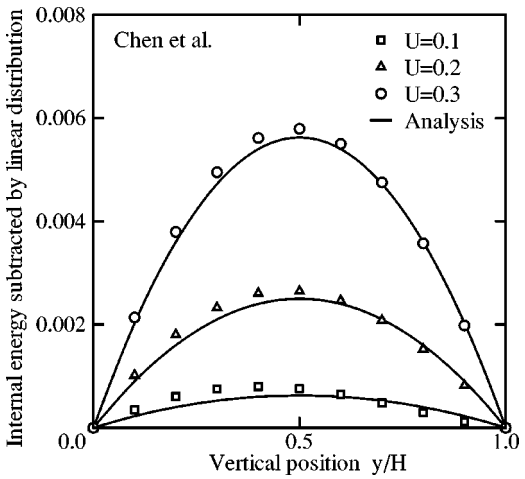

FIG. 13. Chen's model. Internal energy at steady state for different wall temperatures: $e_1=0.3, e_2=0.7$ and $\phi=0.1$. The internal energy subtracted by linear distribution is shown. The wall speed is changed: $U=0.1, 0.2, 0.3$. The model gives distorted solutions.

dependency on the wall temperature, which also contradicts the analysis. Those discrepancies are the reflection of the error terms described above.

The model by Chen *et al.* 2D16V (2 speeds of group I and 2 speeds of group II) [4,7]. They say that as they retain up to fourth orders of local flow speed and realize equivalent up to seventh rank tensor isotropy by mixing weighted group I and group II velocities, their model recovers correct fluid equations.

The result for various values of the relaxation parameter ϕ is shown in Fig. 11. Although Chen's model has been quite improved from Alexander's model, the model still yields an erroneous solution for $\phi<0.2$. For $\phi=0.1$, the result for various values of the wall temperature is shown in Fig. 12. This figure indicates that, for $\phi<0.2$ (low viscosity flow), the simulation yields an erroneous solution if the internal energy e diverts from 0.5. Consequently, the simulation for $e_1\neq e_2$, as shown in Fig. 13, although the average internal energy is 0.5, gives distorted solutions if the difference in temperature between walls exceeds a certain range. Further study are necessary where these discrepancies come from.

VI. CONCLUSIONS

A two-dimensional multispeed thermal model for the FDLBM was proposed. To recover correct fluid equations, up to fourth orders of local flow velocity should be retained in the local equilibrium distribution function and the particle velocities should have up to seventh rank isotropy. In the FDLBM, we can select particle velocities independently from the lattice configuration. Therefore, we adopt particle velocities of octagonal directions, which have up to seventh rank isotropic tensors. We verified the model conducting flow simulations and compared it with the existing models. While the existing multispeed thermal models give correct answers in quite limited ranges of viscosity and internal energy, the model proposed in this paper gives correct answers in wide ranges.

We would like to note that the proposed model has capability in the high Reynolds number problems. In our application study [8], thermal cavity flow simulations of $\phi=0.0009$ was successfully conducted.

[1] S. Chen and G. Doolen, Annu. Rev. Fluid Mech. **30**, 329 (1998).
[2] X. Shan and H. Chen, Phys. Rev. E **47**, 1815 (1993).
[3] F.J. Alexander, S. Chen, and J.D. Sterling, Phys. Rev. E **47**, R2249 (1993).
[4] Y. Chen, H. Ohashi, and M. Akiyama, Phys. Rev. E **50**, 2776 (1994).
[5] N. Cao, S. Chen, S. Jin, and D. Martinez, Phys. Rev. E **55**, R21 (1997).
[6] S. Wolfram, J. Stat. Phys. **45**, 471 (1986).
[7] Y. Chen, H. Ohashi, and M. Akiyama, J. Stat. Phys. **81**, 71 (1995).
[8] M. Watari and M. Tsutahara, in Thermal Cavity Flow of Compressible Fluids. Numerical Simulation by a Newly Proposed Model of Finite Difference Lattice Boltzmann Method, The Fifth JSME-KSME Fluids Engineering Conference Nov. 2002 (unpublished).